Pergamon

Acta Materialia 50 (2002) 2199–2207

Acta MATERIALIA

www.actamat-journals.com

# Computational and experimental investigation of microsegregation in an Al-rich Al–Cu–Mg–Si quaternary alloy

X. Yan [a], S. Chen [b], F. Xie [a], Y.A. Chang [a,*]

[a] *Department of Materials Science and Engineering, University of Wisconsin-Madison, 1509 University Avenue, Madison, WI 53706-1595, USA*

[b] *CompuTherm, LLC, 437 S. Yellowstone Dr., Suite 217, Madison, WI 53719, USA*

Received 23 March 2001; received in revised form 4 July 2001; accepted 4 July 2001

**Abstract**

A new micromodel was developed to predict the microstructure and microsegregation in multicomponent alloys during dendritic solidification. The micromodel was directly coupled with multicomponent phase diagram calculations using a user friendly and robust phase diagram calculation engine—PanEngine. Solid back diffusion, undercooling and coarsening effects were included in this model, and the experimentally measured cooling curves were used as the inputs to carry out the microsegregation calculations. Microsegregation in Al–4.5 wt%Cu–1 wt%Si–0.5 wt%Mg alloy was experimentally investigated from directional solidification and electron probe microanalysis. Calculated results using this model are in accord with the experimental data, while results from the Scheil model deviate significantly from the experimental data. 

*Keywords:* Al–Cu–Mg–Si quaternary alloy; Microsegregation; Solidification; Modeling

## 1. Introduction

The Al–Cu–Mg–Si system is the basis of a large group of cast and wrought aluminum alloys. A basic understanding of the thermodynamics, phase relations, and the solidification behavior of the system is essential in developing new materials, as well as for improving the performance of existing commercial alloys. Meanwhile, microsegregation phenomena are of technical importance since they have implications on the properties of the alloys. For example, the formation of brittle non-equilibrium phases can cause a deterioration in the mechanical properties. Variations of concentration can lead to an inhomogeneous precipitation distribution after a heat treatment and therefore poor fatigue behavior. Segregation can also decrease other physical properties such as corrosion resistance. So, accurate predictions of microsegregation and microstructure in metallic alloys are highly important.

One of the key parameters needed in the micromodeling of solidification of an alloy is the

* Corresponding author. Tel.: +1-608-262-3732; fax: +1-608-262-0389.

*E-mail address:* chang@engr.wisc.edu (Y.A. Chang).

1359-6454/02/$22.00 
PII: S1359-6454(01)00431-1

partition coefficient. However, the partition coefficient as a function of temperature and concentration of alloying elements is usually unknown for multicomponent systems. The common assumption of a constant partition coefficient is not acceptable because the actual value may vary significantly with temperature. Since nearly all commercial alloys have many components, often exceeding five components, there is a strong industrial need to investigate and simulate more complex alloys. In recent years, some investigators have tried to directly couple phase diagram calculation with micromodeling [1–6]. But, this kind of coupling has been restricted to binary [1] and ternary systems [2–6] mainly due to the following two reasons: (1) the lack of an appropriate database; (2) the difficulties in calculating phase equilibria for quaternary and higher order systems using the available phase diagram calculation interfaces. One of the most extensively used micromodels is that developed by Kraft et al. [2], which considered both kinetic and thermodynamic effects. Good agreement was obtained between model calculation and experimental data for ternary systems, such as Al–Cu–Mg [3]. Xie [7] investigated the microstructure and microsegregation in the Al–Cu–Mg–Zn quaternary system by directly coupling Kraft's micromodel with phase diagram calculation through the ThermoCalc interface [8]. Deviation was found between the model-calculated results and the experimental data for each solute near the edge of a dendrite arm. This is because solid back diffusion was not considered at the later stage of solidification since the interface cannot handle the case when the remaining liquid reaches the region where two or more solid phases form simultaneously [7].

More recently, we [9] have developed a new approach to directly couple the microsegregation calculation with phase diagram calculation for multicomponent systems (e.g. seven-component Al–Cu–Mg–Fe–Si–Mn–Zn A319 alloys [10]). Using this approach, the tie lines are calculated every time the kinetic equations are solved during solidification simulation.

In the present study, we intend to couple the phase diagram calculation with a microscopic model for calculating the microsegregation in Al-rich Al–Cu–Mg–Si alloys. This alloy system was chosen because of its technological importance in the automobile and aerospace industries. In the following, we will present: (1) model description, (2) coupling of microscopic modeling with phase diagram calculation, (3) experimental method, (4) results and discussions, and (5) conclusions.

## 2. Model description

The present numerical micromodel predicts the secondary dendrite arm spacing (SDAS), element distribution in the dendrite arms and types and amounts of non-equilibrium phases in the entire range of dendritic solidification in multicomponent alloys. The main thermodynamic and kinetic effects that can influence the solidification behavior are accounted for. The most important extensions as compared to earlier models [1] are: (a) extension to the higher order alloys, (b) direct coupling with multicomponent phase diagram calculation, (c) inclusion of undercooling effects and dendrite arm coarsening for multicomponent alloys, and (d) solid back diffusion during the whole solidification stage.

This numerical micromodel is basically a modified Scheil model [18] incorporating back diffusion, undercooling and dendrite arm coarsening. Three geometric shapes, i.e. plate, cylinder and sphere, were used to describe the growing secondary or tertiary arms. Because of the symmetry of the dendrite arms there is no mass flow through the center of the arm and therefore only one half of the arm is considered. Coarsening of the dendrite arms during solidification is taken into account by increasing the length of the volume element with time. Beaverstok's model [11], which takes into consideration all solute elements for the multicomponent system instead of only the element with the lowest value of coarsening parameter [12], was used for the calculation of coarsening. A total of five different possible contributions to the undercooling were considered [13]: solutal undercooling, curvature undercooling, temperature gradient undercooling, kinetic undercooling, and solute trapping. Only the solutal and gradient undercoolings play an important role under the

conditions of the experiments carried out in the present study. Diffusion in the liquid is assumed to be so rapid that the liquid concentration is essentially uniform. For an *n*-component system, back diffusion in (α-Al) phase was obtained by solving the multicomponent form of Fick's second law numerically:

$$\frac{\partial^2}{\partial x^2}([D_{ij}]C_j) = \frac{\partial}{\partial t}(C_i),(i = 1,2,\ldots,n-1) \quad (1)$$

Where $i$ and $j$ stand for $i$th and $j$th component, respectively. In the diffusivity matrix $[D_{ij}]$, all the off-diagonal terms were assumed to be zero. The diagonal terms, $D_{ii}$, follow a standard Arrhenius law [14]:

$$D_{ii} = D_i^0 \exp(-\frac{Q_i}{RT}) \quad (2)$$

where $D_i^0$ is a frequency factor term, $Q_i$ the molar activation energy for diffusion and $R$ is the gas constant. In addition to the diffusion coefficients, other physical properties, such as surface tension, density, and latent heat are also needed. The physical properties needed are listed in Table 1. The liquid diffusion coefficients, which are required for the calculation of dendrite arm coarsening [9–12] and dendrite tip undercooling [13], are also presented in Table 1.

The computational flow chart is shown in Fig. 1. After some initialization steps (such as reading the physical data, cooling rate), the dendrite tip undercooling $\Delta T_T$ are determined. Once the growth parameters are defined, the actual microsegregation calculation is started. The subsequent temperature step $\Delta T^i$ is predefined by user and automatically

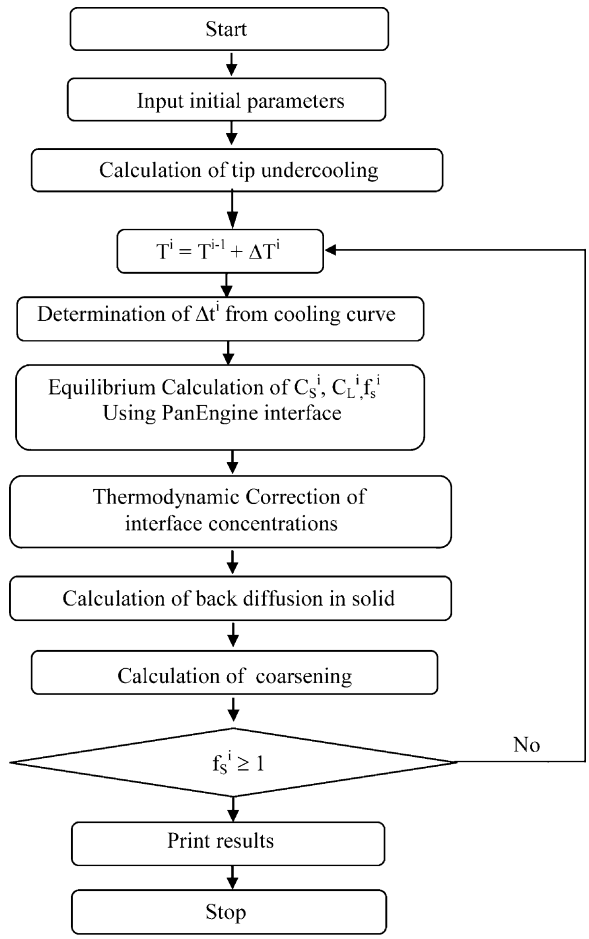


Fig. 1. Flow chart of the numerical computation.

Table 1
Physical and thermal data for Al–Cu–Mg–Si alloys used in the model calculations

| | | |
|---|---|---|
| Liquid diffusion coefficient of Cu | $D_L^{Cu} = 1.05 \times 10^{-7}\exp(-2856/T)\text{m}^2/\text{s}$ | [19] |
| Solid diffusion coefficient of Cu | $D_S^{Cu} = 4.8 \times 10^{-5}\exp(-16{,}069/T)\text{m}^2/\text{s}$ | [20] |
| Liquid diffusion coefficient of Mg | $D_L^{Mg} = 9.90 \times 10^{-5}\exp(-8610/T)\text{m}^2/\text{s}$ | [21] |
| Solid diffusion coefficient of Mg | $D_S^{Mg} = 6.23 \times 10^{-6}\exp(-13{,}831/T)\text{m}^2/\text{s}$ | [22] |
| Liquid diffusion coefficient of Si | $D_L^{Si} = 0.08 \times 10^{-7}\exp(-2856/T)\text{m}^2/\text{s}$ | [22] |
| Solid diffusion coefficient of Si | $D_S^{Si} = 2.02 \times 10^{-4}\exp(-16{,}069/T)\text{m}^2/\text{s}$ | [22] |
| Energy of solid–liquid interface | $\gamma = 0.093\text{J}/\text{m}^2$ | [19] |
| Specific latent heat of solidification | $\Delta h = 9.5 \times 10^8\text{J}/\text{m}^3$ | [23] |
| Geometric factor for coarsening | $G = 35$ | [23] |

adjusted by the program in order to find all phase equilibria during solidification. The corresponding time step $\Delta t^i$ can be obtained with the cooling curve and temperature step $\Delta T^i$. The effects of cooling rate, dendrite arm coarsening and back diffusion in the solid are calculated in the loop. A recently developed quaternary Al–Cu–Mg–Si thermodynamic description [9] has been used for phase diagram calculation in this study. The numerical computation is fully coupled with a robust, user-friendly multicomponent phase equilibrium calculation Engine—PanEngine [16], which will be introduced in Section 3.

## 3. Coupling micromodeling with phase diagram calculation

Modeling of solidification relies on phase equilibrium information describing the solid–liquid interface. Incorrect assumptions concerning the phase diagram can easily lead to erroneous predictions. The best and most accurate method for treating the phase equilibrium at the interface is to couple the microsegregation calculation with phase diagram calculations according to the CALPHAD method [15].

To implement the phase equilibria calculation in micromodeling, the multicomponent phase diagram calculation interface-PanEngine was used [16]. This interface was developed by CompuTherm LLC and is the core component of the phase diagram calculation software—PANDAT. PanEngine has the ability to solve the phase equilibrium when liquid phase reaches the region where two or more solid phases form simultaneously. Fig. 2 shows schematically the coupling of micromodeling with phase diagram calculation. PanEngine calculates the tie lines in the multicomponent system at each time step of the solidification process. As shown in Fig. 1, phase equilibrium at the interface was calculated using the average composition of the remaining liquid from the previous time step as the overall liquid composition in the current time step; then the kinetic and thermodynamic effects, such as thermodynamic correction of the interface concentration, solid-back diffusion and secondary arm spacing, were considered. Mass balances for all components were maintained during each step. Phase fractions formed in current step and the concentration change in the (Al) phase were thus obtained. The composition of the remaining liquid was fed back to the PanEngine interface to carry out the equilibrium calculation for the next time step. The phase fractions, SDAS and solute concentration in the (Al) phase were output into a datafile. The output datafile also included heat evaluation, fs–$T$ relationship, solidification path, (liquid concentration versus temperature) and equilibrium and non-equilibrium partition coefficients for all the components.

## 4. Experimental method

The directional solidification apparatus used in the present study and shown in Fig. 3 consists of a vertical resistance furnace, a position table coupled with a microstep motor, and a computer controlled indexer. An alumina tube with an inside diameter of 3 cm and a length of 40 cm was placed inside this resistance furnace with three heating zones; each of which can be controlled separately. A water-cooling jacket was placed at the bottom of the furnace in order to control the unidirectional solidification of the melt. An alumina tube with 3 mm ID, 4.5 mm OD and 350 mm in length containing the alloy specimen to be solidified was inserted through the cooling jacket. Its position is fixed by a sample holder with about 25 cm of its length exposed to the hot zone and the remaining 10 cm to the cold zone. The specimen can be moved with speeds varying between 0.2 μm/s and 40 mm/s. Each of the Al–4.5Cu–1Si–0.5Mg (wt%, base of A2214 alloy) samples, obtained from a master alloy prepared by casting at the Alcoa Technical Center, was melted and then evacuated in the 3 mm ID alumina tube in the directional solidification apparatus.

A thermocouple was inserted into the sample inside the 3 mm ID alumina tube from the top of the furnace after the top part of the sample was completely molten in order to monitor the thermal profile within the sample during solidification. The EMF produced by the thermocouple was measured and recorded by an accurate temperature acqui-

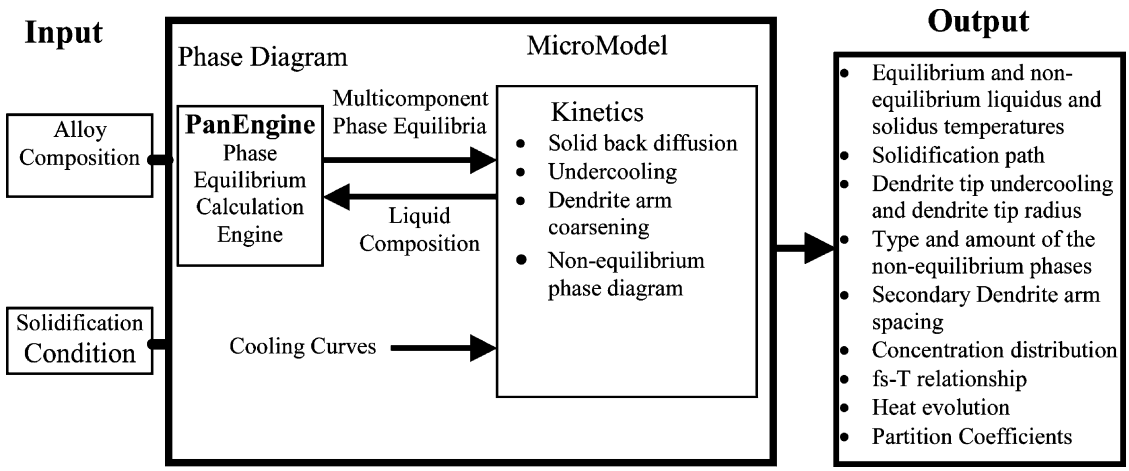


Fig. 2. A schematic diagram of micromodeling.

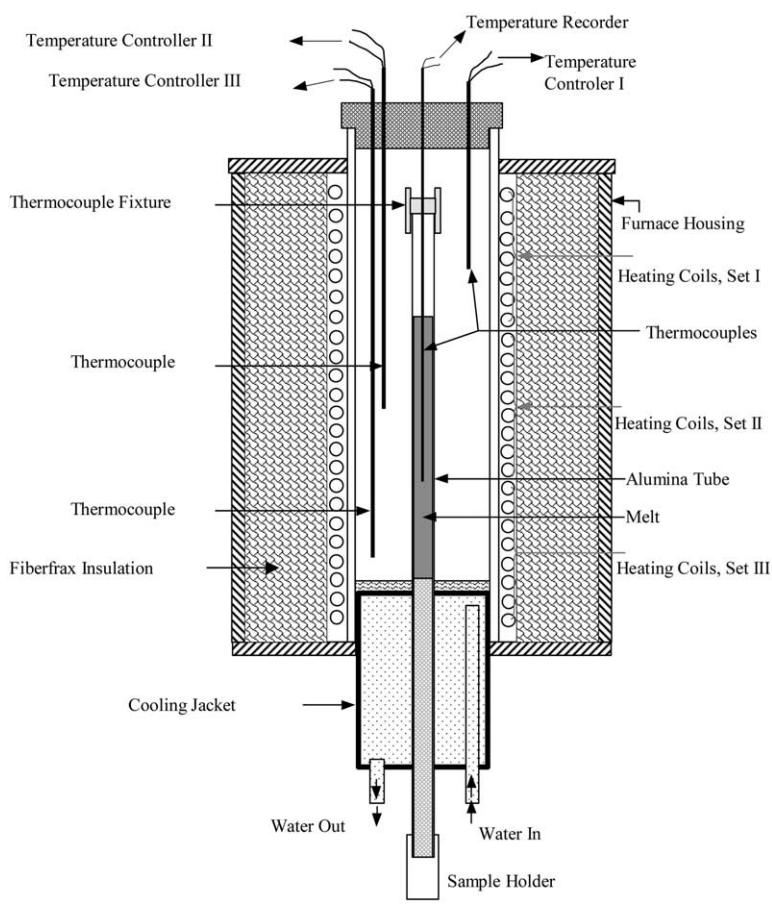


Fig. 3. A schematic diagram of the directional solidification system.

sition system (NI4300, National Instruments). The temperature profile recorded for each sample during solidification was used as the input *cooling curve T* (*time*) for calculating the degree of microsegregation as presented later.

Each of the alloy specimens was superheated to about 100 °C above the liquidus temperature for 1 h prior to the start of directional solidification. The sample was solidified for about 10–15 cm at a predetermined rate with thermal gradients kept at about 50 °C/cm near the solid–liquid interface; after which the sample was quenched in a water–ice mixture. Each of the solidified samples was transversely cross-sectioned and polished but not etched. Composition measurements and microstructure analysis were carried out using a fully automated Cameca SX-50 scanning electron microprobe. The composition measurements were carried out using a wavelength dispersive spectrum method (WDS). Pure Al, Cu, Si and MgO were used as the standards. A total of 400 measurements were carried out automatically over an area of $800 \times 800\mu m^2$**.** These measured data were analyzed and compared with the calculated values.

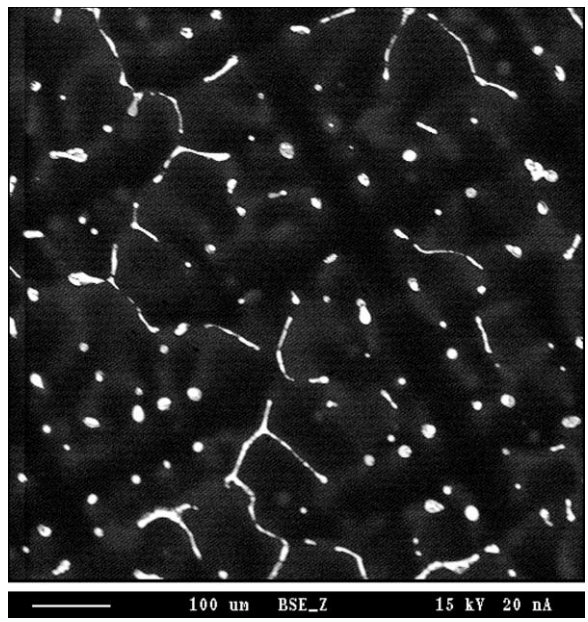


Fig. 4. Typical dendrite structure in transverse section of the directionally solidified Al–4.5Cu–1Si–0.5Mg alloy at a growth rate of 0.05 mm/s with a temperature gradient of 50 K/cm at the liquid–solid interface.

## 5. Results and discussion

A quaternary Al–4.5Cu–1Si–0.5Mg alloy was solidified in the present study with the solidification rates of 0.013, 0.050 and 0.15 mm/s under a temperature gradient of 50 K/cm. The microstructures of the solidified samples are dendritic. A typical dendrite microstructure of the directionally solidified alloy samples is shown in Fig. 4. In this BSE image, the dark areas are (Al) (aluminum phase) and the bright areas are $\theta$ (the $Al_2Cu$ phase) and eutectic mixtures. The ternary and quaternary eutectic mixtures consist of (Al), $\theta$, Si and $Q$-$Al_5Cu_2Mg_8Si_6$. The different gray scales show varying solute content in the primary (Al) phase, indicating the main growth directions of the secondary dendrite arms. The primary stem is located at the junction of two secondary arms.

The area scan method was used to measure the microsegregation in the quaternary Al–4.5Cu–0.5Mg–1Si alloy solidified with three growth rates of 0.013, 0.05 and 0.15 mm/s with a temperature gradient of 50 K/cm. Fig. 5 (a)–(c) shows the measured solute concentration on $800 \times 800\mu m^2$ area of the sample solidified at a growth rate of 50 μm/s. High Cu concentration areas in Fig. 5(a) correspond with the formation of $\theta$-$Al_2Cu$, and high Si concentration areas in Fig. 5(b) correspond with the formation of the (Si) phase, while the high Mg concentration areas in Fig. 5(c) correspond with the formation of $Q$-$Al_5Cu_2Mg_8Si_6$ phase. The calculated solidification path of this alloy under the present solidification condition includes:
(1)L→(Al);(2)L→(Al) + (Si);(3)L→(Al) + (Si) + $\theta$and(4)L→(Al) + (Si) + $\theta$ + $Q$. Since the $Q$-$Al_5Cu_2Mg_8Si_6$ phase precipitates only at the final stage of solidification in quaternary eutectic mixtures (Al + Si + $\theta$ + $Q$), the areas with high Mg content in Fig. 5(c) are also the high Si and high Cu concentration areas as shown in Fig. 5(b) and (a).

In order to obtain the composition versus fractions of solids profile, the same approach as used by Lacaze and Lesoult [17] was applied in this study. The measured solute distributions of Cu at

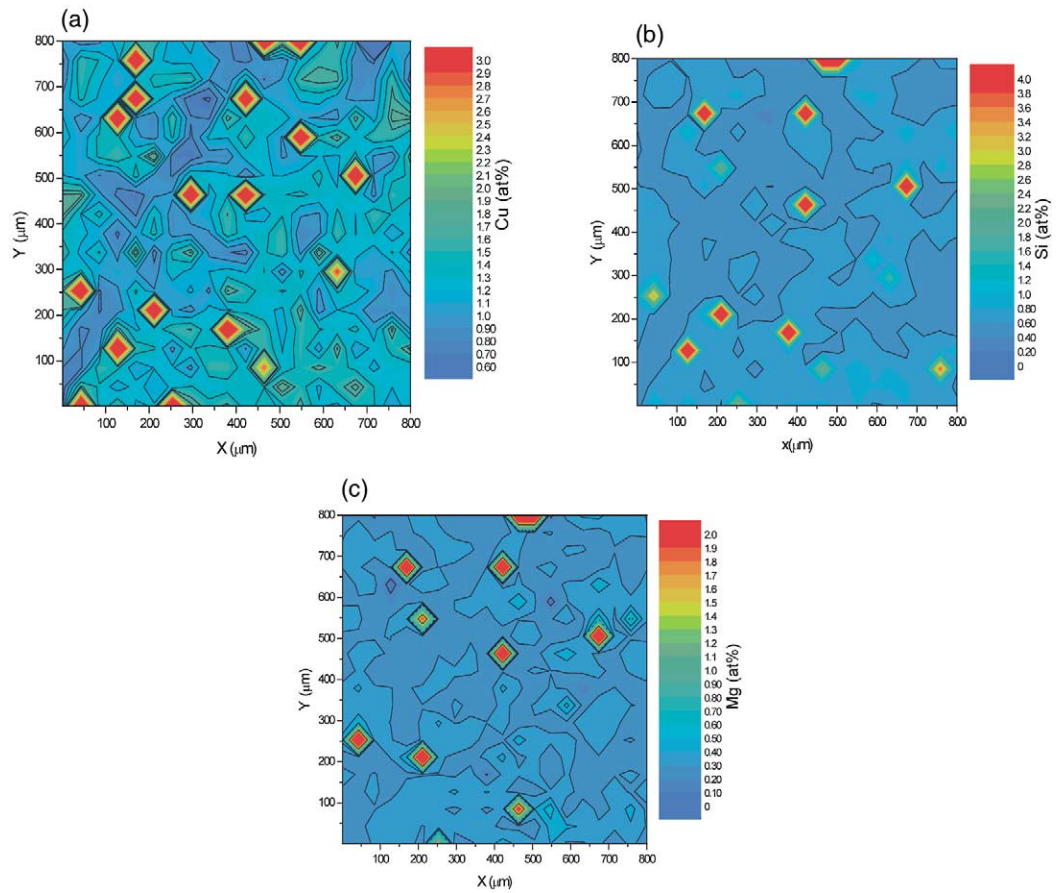


Fig. 5. (a) Experimentally determined Cu concentration contour plot in directionally solidified Al–4.5Cu–1Si–0.5Mg (wt%) alloy at a growth rate of 0.05 mm/s with a temperature gradient of 50 K/cm. (b) Experimentally determined Si concentration contour plot in directionally solidified Al–4.5Cu–1Si–0.5Mg (wt%) alloy at a growth rate of 0.05 mm/s with a temperature gradient of 50 K/cm. (c) Experimentally determined Mg concentration contour plot in directionally solidified Al–4.5Cu–1Si–0.5Mg (wt%) alloy at a growth rate of 0.05 mm/s with a temperature gradient of 50 K/cm.

growth rate of 0.013 and 0.05 mm/s with a temperature gradient of 50 K/cm are shown in Figs. 6 and 7. The measured solute distributions of Si and Mg at a growth rate of 0.15 mm/s with a temperature gradient of 50 K/cm are shown in Fig. 8.

Three dendrite arm geometries, plate, cylinder and sphere, were considered in the micromodel, and the calculated results, as shown in Figs. 6 and 7, were compared with those obtained under Scheil conditions and with the experimental data. It is evident from these figures that the calculated concentration gradients using the Scheil model [18] are not adequate. Although the calculated values using the modified Scheil model improves irrespective of the geometries used to approximate the shapes of the dendrites, the spherical model yields values in best agreement with the experimental data. The agreement is good initially at small fractions of solids but deviations occur at higher fractions of solids. On the contrary, the calculated values using the cylindrical geometry are in better accord with the experimental data at higher fractions of solids. Similar results were obtained for Si and Mg concentrations. As shown in Fig. 8, the calculated Si and Mg concentration profiles using the spherical model are in agreement with the experimental data.

The volume fractions of the (Al) phase in the solidified structures were measured by automatic

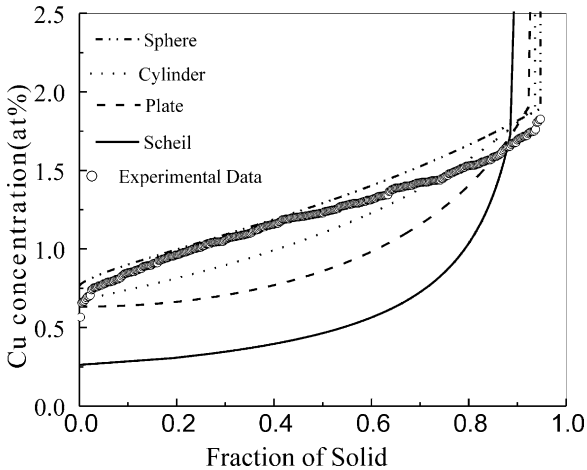


Fig. 6. Cu concentration profile in the primary dendrites as a function of the fractions of solid: comparison between the model-calculated values and experimental data for a growth rate of 0.013 mm/s and a temperature gradient of 50 K/cm at the liquid–solid interfaces.

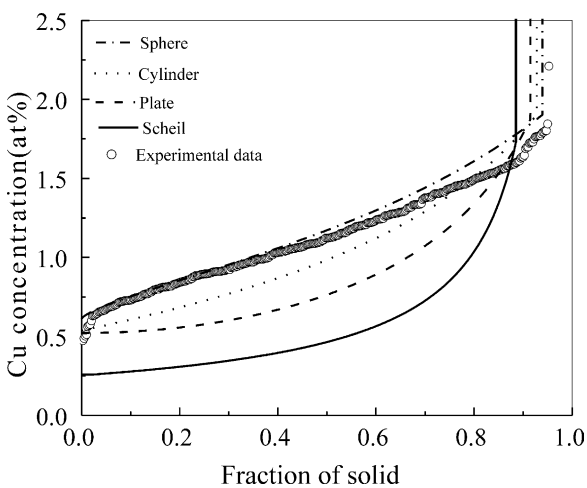


Fig. 7. Cu concentration profile in the primary dendrites as a function of the fractions of solid: comparison between the model-calculated values and experimental data for a growth rate of 0.05 mm/s and a temperature gradient of 50 K/cm at the liquid–solid interfaces.

image analysis of the BSE images, and given in Table 2. The measured (Al) phase includes both primary and secondary (Al) since secondary (Al) in the binary eutectic forms on the surface of primary dendrites. As can be seen in Table 2, the volume fractions of the (Al) phase increase with increasing

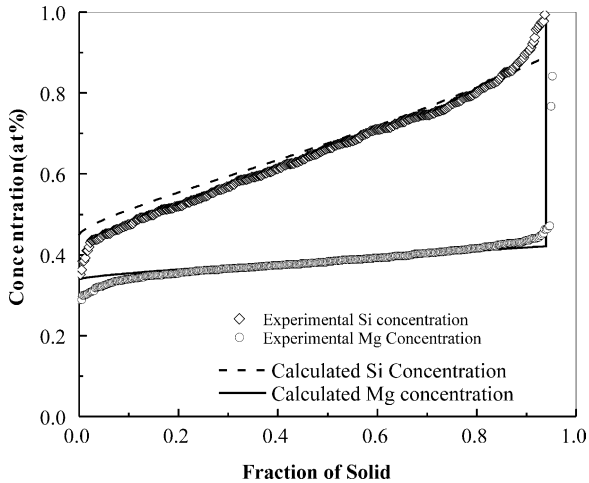


Fig. 8. Mg and Si concentration profiles in the primary dendrites as a function of the fraction of solid: comparison between the model-calculated values and experimental data for a growth rate of 0.15 mm/s and a temperature gradient of 50 K/cm at the liquid–solid interface.

growth rate. The average dendrite arm spacing $\lambda_2$ measured from the BSE images are also listed in Table 2, and it can be seen that it increases as the growth rate decreases. The fractions of (Al) calculated under the Scheil conditions and calculated using the spherical model at different cooling rates are also given in Table 2. The fraction of (Al) with Scheil conditions is less than the measured values while those calculated from the present micromodel are in accord with the measured ones as shown in Table 2. The calculated dendrite arm spacings for the quaternary alloy studied are also in agreement with the measurements.

## 6. Conclusions

Microsegregation in a quaternary Al-rich Al–4.5Cu–0.5Mg–1Si (wt%) alloy was investigated experimentally using directional solidification at growth rates varying between 0.013 and 0.5 mm/s with a temperature gradient of 50 K/cm. A reliable area scan method was used for obtaining the solute distributions.

A microscopic model was directly coupled with multicomponent phase diagram calculation in present study. The multicomponent phase diagram

Table 2
Comparison of experimental and calculated phase fractions and dendrite arm spacings $\lambda_2$

| Growth rate (mm/s) | $\lambda_2$ (μm) | | Amount of primary (Al) (vol.%) | | | |
|---|---|---|---|---|---|---|
| | Image analysis | Model calculation | Area scan | Image analysis | Model calculation | Scheil model |
| 0.013 | 120 | 122.3 | 95 | 96 | 95.1 | 88.45 |
| 0.05 | 67 | 66.6 | 95.25 | 96.5 | 95.5 | 88.45 |
| 0.15 | 46 | 45.1 | 96.25 | 96.7 | 95.7 | 88.45 |

calculation interface-PanEngine was used for the phase equilibrium calculations. Back diffusion in the solid, undercooling and dendrite arm coarsening were considered in the micromodel. While the calculated values using the Scheil model deviate significantly from the experimental data, those using the present model are in better agreement with the experimental data. Among the three geometrical models, i.e. plate, cylinder and sphere, agreement is the best when the sphere is used to approximate the shapes of the dendrite arms.

The microscopic model is a powerful tool for predicting the solidification path and microsegregation in multicomponent ($>5$ components) aluminum alloys under different cooling rates and for selecting the cooling conditions for microstructure control.

## Acknowledgements

We wish to thank the National Science Foundation for financial support through grant No. NSF-DMR-94-21780, and Dr Bruce MacDonald of the Metal Program of the Materials and Processing Cluster of NSF for his interest. We also wish to thank Dr M. Chu and Alcoa Technical Center, Aluminum Company of America, for providing us the cast alloy used in this study.

## References

[1] Kraft T, Chang YA. JOM 1997;49:20.
[2] Kraft T, Rettenmayr M, Exner HE. Model Simul Sci Eng 1996;4:161.
[3] Xie F-Y, Kraft T, Zuo Y, Moon C-H, Chang YA. Acta mater 1999;47:489.
[4] Borgenstam A, Engstrom A, Hoglund L, Agren J. J Phase Equilibria 2000;21:269.
[5] Byeong-Joo Lee. Script mater 1999;40:573.
[6] Dore X, Combeau H, Rappaz M. Acta mater 2000;40:3951.
[7] Xie F-Y. PhD thesis. University of Wisconsin-Madison; 1999.
[8] Sundman Bo, Chen Qing. Thermodynamic calculation interface (TQ)-programmer's guid. Sweden: Royal Institute of Technology, 1997.
[9] Yan X-Y. PhD thesis. University of Wisconsin-Madison; 2001.
[10] Yan X-Y, Ravi Vijayaraghavan, Chang YA. Technical report: predicting microstructure and microsegregation in 319 alloys. Ford Motor Company; 2000.
[11] Beaverstock RC. In: Beech J, Jones H, editors. Solidification processing 1997. Sheffield, UK: Department of Engineering Materials, University of Sheffield; 1997. p. 321.
[12] Roosz A, Exner HE. Acta Metall Mater 1990;38:375.
[13] Yan X-Y, Xie F-Y, Chu M, Chang YA. Mater Sci Eng A 2001;302:268.
[14] Eden Glicksman Martin. Diffusion in solids. New York: Wiley, 2000.
[15] Kaufman L, Bernstein H. Computer calculation of phase diagrams. New York: Academic Press, 1970.
[16] Chen S-L, Daniel S, Zhang F, Chang YA, Oates WA, Schmid-Fetzer R. PanEngine 1.0-phase equilibrium calculation engine for multicomponent systems. Madison, WI: Computherm LLC, 2000.
[17] Lacaze J, Lesoult G. ISIJ Int 1995;35:658.
[18] Scheil E. Z Metallk 1941;34:70.
[19] Roosz A, Halder E, Exner HE. Mater Sci Technol 1986;2:1149.
[20] Bergner D. Neue Hütte 1984;29:207.
[21] Kovacova K, Grman D. Kovove mater 1979;17:144.
[22] Brandes EA. In: Brook GB, editor. Smithells metals reference book. 7 ed. Springer Verlag: Berlin, Heidelburg; 1992.
[23] Kurz W, Fisher DJ. In: Fundamentals of solidification. 3rd ed. Aedermannsdorf, Switzerland: Trans Tech Pub; 1989. p. 29-3.